Transactions on Computer Science and Intelligent Systems Research
ISSN: 2960-1800, eISSN: 2960-2238 | Volume 11
TPCEE 2025

Lorentz Force Damping Mechanism in Non-Uniform Magnetic Fields and Its Application in Vibration Isolation

Zian Huang *
Shanghai Songjiang No.2 High School, Shanghai 201600, China
* Corresponding Author Email: 18221302561@163.com

Abstract. This study delves deeply into the theoretical basis of the Lorentz force damping mechanism in non-uniform magnetic fields and its application potential in the field of vibration isolation. By establishing the dynamic model of the rectangular coil in the gradient magnetic field and combining it with the numerical simulation system, the nonlinear enhancement relationship between the magnetic field gradient and the damping performance was analyzed. The research verified the significant strengthening effect of the magnetic flux change rate of the gradient magnetic field on the damping effect, revealing that increasing the magnetic field gradient can effectively enhance the system response speed and vibration suppression capability, while reducing the circuit resistance further optimizes the energy dissipation efficiency. In the extended model, the synergistic effect of position-dependent nonlinear damping force and elastic restoring force has been systematically analyzed. This technology offers an innovative solution for vibration control in the industrial field.

Keywords: Lorentz Force Damping; Non-uniform Magnetic Fields; Vibration Isolation; Gradient Magnetic Field Optimization.

1. Introduction

Against the backdrop of the rapid development of technology today, the requirements for vibration control in precision equipment are constantly rising to unprecedented heights (Dai et al., 2023).

The continuous innovation of semiconductor manufacturing processes, the major breakthroughs in space exploration technologies, and the in-depth development of life science research have significantly increased the sensitivity of various high-end equipment to environmental vibrations (Huang et al., 2021; Zhou et al., 2022). The requirements for vibration control of advanced equipment such as extreme ultraviolet lithography systems and gravitational wave detectors have approached the physical limit, which poses a severe test to traditional vibration isolation technologies (Smith et al., 2023). Although the traditional passive vibration isolation system has the advantages of simple structure and reliable operation, its effect is not good when dealing with low-frequency vibration (Shahzad et al., 2024). Its vibration isolation performance will be significantly reduced, and at the same time, a significant vibration amplification phenomenon will occur in the resonance region (Zhou et al., 2022; Liu et al., 2024). It is particularly worth noting that even for the most basic vibration isolation components, minor design adjustments can cause significant changes in performance parameters (Liu et al., 2024), which fully demonstrates the technical complexity in the field of vibration control (Bhat et al., 2025).

To break through the limitations of traditional technologies, active control technology based on electromagnetic principles has opened up a new research direction (Tumse et al., 2022). The magnetic levitation vibration isolation system, with its non-contact characteristics, effectively avoids mechanical friction and wear problems and shows unique advantages under extreme working conditions (Huang et al., 2021). Among them, the Lorentz force control technology generates precise damping force through the dynamic interaction between the magnetic field and the conductor, demonstrating outstanding response speed and control accuracy (Cheng et al., 2025). Innovative system design schemes, such as the combined application of magnetic levitation gravity compensators and Lorentz force motors, have achieved remarkable results in vibration control with nanoscale precision (Meng et al., 2024). Researchers have made significant progress in vibration isolation experiments in a microgravity environment by establishing multi-degree-of-freedom dynamic models and integrating intelligent control algorithms (Zhou et al., 2021), and these breakthroughs provide new technical ideas for vibration control of ultra-precision equipment (Zhang et al., 2023).

As research delves deeper into the field of non-uniform magnetic fields, the Lorentz force damping mechanism demonstrates more abundant physical properties and application prospects. In this special magnetic field environment, the damping effect exhibits characteristics that are completely different from those of a uniform magnetic field (Ballicchia et al., 2024). By optimizing the magnetic circuit design, efficient dissipation of vibration energy can be achieved. The system design that combines negative stiffness elements with Lorentz force damping can simultaneously meet the requirements of high static stiffness and quasi-zero dynamic stiffness (Shahraeeni, 2023). The latest research adopted a specially designed symmetrical structure and successfully simulated the nonlinear damping behavior with memory characteristics, which demonstrated outstanding vibration suppression performance over a wide frequency range (Ma & Yan, 2021). These research achievements not only deepen our understanding of vibration control theory, but also provide innovative solutions to the vibration control problems in the field of cutting-edge science and technology (Wilson et al., 2023).

A thorough analysis of the advantageous features of this new type of damping mechanism reveals that it possesses multiple technical highlights and unique values (Li et al., 2025). The non-contact working mode fundamentally eliminates the problem of mechanical wear (Huang et al., 2021), greatly extends the service life of equipment, and significantly reduces maintenance costs at the same time; The flexible adjustability enables it to adapt to the demands of various complex working conditions by changing the excitation current or the spacing of permanent magnets (Huang et al., 2021); Outstanding wideband suppression capability (Shahraeeni, 2023); Combined with a compact structural design (Ma & Yan, 2021), it demonstrates unique value in space-constrained application scenarios. From 7nm chip Manufacturing to Space Gravitational Wave detection (Meng et al., 2024; Zhou et al., 2021), from High-Speed trains to intelligent robots (Niu & Chen, 2021; Huang et al., 2023, and then to kilometer-level super high-rise buildings and cross-sea bridge projects (Lei et al., 2017; Huang et al., 2021). This innovative technology is leading profound changes in the field of vibration control and promoting technological upgrading in related industries.

Although significant progress has been made in current research in magnetic field optimization and system design (Ballicchia et al., 2024), there are still many challenges and unsolved problems to achieve a comprehensive breakthrough in technology. This paper breaks through the traditional research paradigm of uniform magnetic fields and focuses on the nonlinear damping characteristics and control mechanism of Lorentz forces in non-uniform magnetic fields. The core innovation points include: establishing an accurate mathematical model of Lorentz force damping in non-uniform magnetic fields, revealing the quantitative relationship between magnetic field gradients and damping effects; A vibration control strategy based on magnetic field configuration optimization is proposed to achieve wideband vibration suppression and explore its engineering applicability. By systematically studying the influence law of magnetic field gradient on damping characteristics, developing new magnetic circuit design schemes, and combining intelligent control algorithms to achieve precise regulation of damping force, this research is dedicated to promoting the development of non-uniform magnetic field Lorentz force damping technology, providing more efficient and reliable vibration isolation solutions for various precision systems. Meanwhile, the research will also focus on thermal management issues, electromagnetic compatibility design, and cost control strategies in engineering applications to ensure that technological achievements can be smoothly transformed into actual productive forces and serve the country's major strategic needs and industrial development.

2. Lorentz force and the theory of non-uniform magnetic field damping mechanism

2.1. The Fundamental Theory of Lorentz Forces

The Lorentz force, as a fundamental concept in electromagnetism, can be deeply explored in terms of its physical connotations from both micro and macro perspectives. At the microscopic level, the motion of a single charged particle in an electromagnetic field follows the fundamental Lorentz force equation:

$$\mathbf{F} = q(\mathbf{E} + \mathbf{v} \times \mathbf{B}) \tag{1}$$

This equation reveals the combined action mechanism of electric and magnetic fields on charged particles. Among them, the electric field force component is independent of the particle's motion state, while the magnetic field force component must depend on the particle's motion speed. This characteristic leads to many interesting physical phenomena.

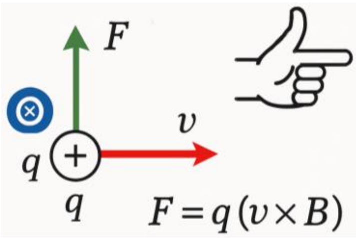

Figure 1. Schematic diagram of Lorentz force principle

In macroscopic engineering applications, we pay more attention to the Lorentz force acting on the current in conductors. By converting the discrete charge motion into a continuous current model, the expression of the Lorentz force acting on the current element can be obtained:

$$\boldsymbol{d}\mathrm{F} = \boldsymbol{Id}\mathrm{l} \times \mathbf{B} \tag{2}$$

This formula holds a core position in the design of magnetic levitation systems. By precisely controlling the current distribution in the conductor or the spatial arrangement of permanent magnets, a resultant force of Lorentz force in a specific direction can be generated (Meng et al., 2024; Ohji et al., 2007). In practical applications, the components of the electrostatic field are usually negligible, which makes the magnetic field the main parameter of the control system. It is worth noting that the direction of the Lorentz force follows the right-hand rule, a characteristic that is crucial in engineering design as it allows for precise control of the direction by adjusting the direction of the current or the magnetic field.

2.2. Characteristics and Mathematical Representation of Non-uniform Magnetic Fields

In real engineering, magnetic fields often have significant spatial non-uniformity, which has a significant impact on the electromagnetic damping effect. Magnetic induction intensity, as a function of spatial position, can be expressed as

$$\mathbf{B} = \mathbf{B}(\mathbf{r}) = \boldsymbol{B_x}(\boldsymbol{x},\boldsymbol{y},\boldsymbol{z})\hat{\imath} + \boldsymbol{B_y}(\boldsymbol{x},\boldsymbol{y},\boldsymbol{z})\hat{\jmath} + \boldsymbol{B_z}(\boldsymbol{x},\boldsymbol{y},\boldsymbol{z})\widehat{\boldsymbol{k}} \tag{3}$$

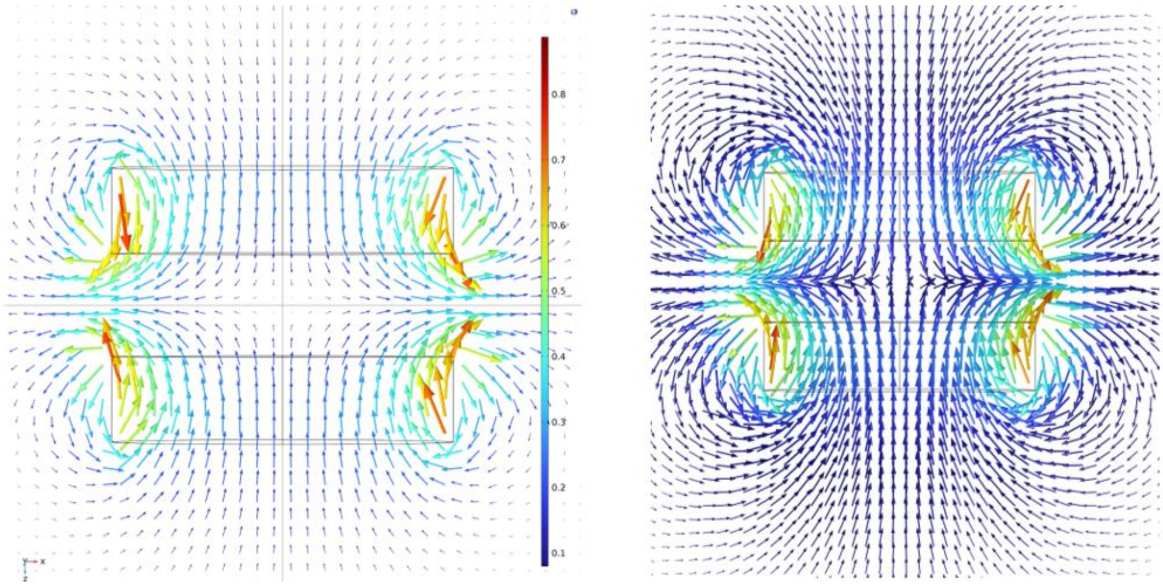

Figure 2. Magnetic field line distribution between repelling magnets

The quantitative description of magnetic field non-uniformity requires the introduction of a magnetic field gradient tensor:

$$\nabla \mathbf{B} = \begin{bmatrix} \frac{\partial B_x}{\partial x} & \frac{\partial B_x}{\partial y} & \frac{\partial B_x}{\partial z} \\ \frac{\partial B_y}{\partial x} & \frac{\partial B_y}{\partial y} & \frac{\partial B_y}{\partial z} \\ \frac{\partial B_z}{\partial x} & \frac{\partial B_z}{\partial y} & \frac{\partial B_z}{\partial z} \end{bmatrix} \tag{4}$$

Each component of this second-order tensor represents the rate of change of the magnetic field in the corresponding direction (Ballicchia et al., 2024). When a conductor moves in such a non-uniform magnetic field, two electromagnetic effects will be produced simultaneously: the moving electromotive force and the induced electromotive force. The moving electromotive force originates from the conductor cutting the magnetic field lines.

$$\mathcal{E}_{\mathbf{mot}} = \int (\mathbf{v} \times \mathbf{B}) \cdot d\mathbf{l} \tag{5}$$

The induced electromotive force is caused by the variation of the magnetic field over time:

$$\mathcal{E}_{\mathbf{ind}} = -\frac{\partial}{\partial t} \iint \mathbf{B} \cdot d\mathbf{A} \tag{6}$$

These two kinds of electromotive forces jointly determine the total induced electromotive force in the conductor, and thereby affect the magnitude and distribution of the induced current (Ohji et al., 2007; Lyu et al., 2017).

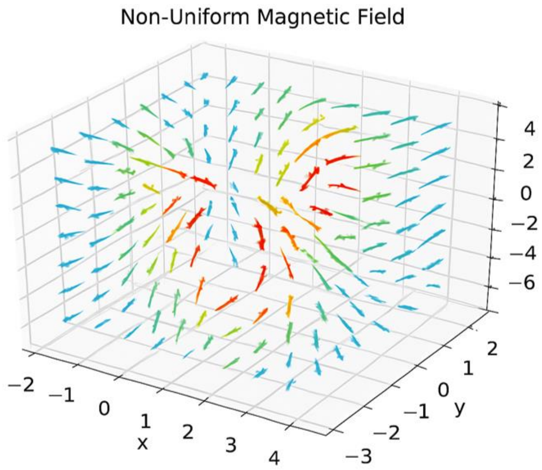

Figure 3. Three-dimensional visualization of the non-uniform magnetic field distribution

2.3. Damping Force Generation and Physical Mechanism

Conductors moving in a non-uniform magnetic field will generate induced electromotive forces due to changes in magnetic flux.

$$\boldsymbol{\mathcal{E}} = -\frac{d\boldsymbol{\Phi}_B}{dt},\ \boldsymbol{\Phi}_B = \iint_S \mathbf{B} \cdot d\mathbf{A} \tag{7}$$

This induced electromotive force will form an induced current in the closed circuit:

$$\boldsymbol{I}_{ind} = \frac{\boldsymbol{\mathcal{E}}}{\boldsymbol{R}} = -\frac{1}{\boldsymbol{R}}\frac{d\boldsymbol{\Phi}_B}{dt} \tag{8}$$

For non-closed conductors, the distribution of this induced current needs to be described by the eddy current density:

$$\nabla \times \mathbf{J}_{\mathrm{eddy}} = -\boldsymbol{\sigma}\frac{\partial \mathbf{B}}{\partial t} \tag{9}$$

These induced currents interact with the original magnetic field, generating a secondary Lorentz force:

$$d\mathbf{F}_{\mathrm{d}} = \boldsymbol{I}_{\mathrm{ind}}\, d\mathbf{l} \times \mathbf{B} \tag{10}$$

$$d\mathbf{F}_{d} = \mathbf{J}_{\mathrm{eddy}} \times \mathbf{B}dV \tag{11}$$

According to Lenz's law, the direction of this force always hinders the movement of the conductor, thereby forming a damping effect. For one-dimensional simple harmonic vibration systems, when the magnetic field gradient remains constant within a certain range, a linear relationship model between damping force and velocity can be established:

$$\boldsymbol{F}_d = -\boldsymbol{c}\boldsymbol{v}_x,\ \boldsymbol{c} \propto \left(\frac{\partial \boldsymbol{B}_z}{\partial x}\right)^2 \frac{L^3}{\rho_e} \tag{12}$$

Here, c represents the damping coefficient, L is the characteristic size of the conductor, and ρ is the resistivity. This model reveals the quadratic enhancement effect of gradient magnetic field intensity on damping performance.

2.4. Energy Dissipation Path

During the electromagnetic damping process, kinetic energy is mainly dissipated through two paths: work done by the Lorentz force and Joule heat dissipation. The calculation formula for Joule thermal power is:

$$\boldsymbol{P_J} = \boldsymbol{I}_{\text{ind}}^{\mathbf{2}}\boldsymbol{R} = \iiint_V \frac{|\mathrm{J_{eddy}}|^2}{\sigma} \boldsymbol{dV} \tag{13}$$

From the perspective of energy conservation, the change in the mechanical energy of a system can be expressed as:

$$\frac{d}{dt}\left(\frac{1}{2}\boldsymbol{mv^2}\right) = \mathbf{F}_d \cdot \mathbf{v} - \boldsymbol{P_J} \tag{14}$$

The first term on the right represents the work done by the Lorentz force, and the second term represents the Joule heat dissipation. For non-ferromagnetic material conductors, Joule heat dissipation accounts for the vast majority of the total energy dissipation, which enables us to enhance the damping efficiency by optimizing the conductivity and geometry of the conductor.

3. Theoretical Models and Numerical Simulations

3.1. Physical Model Construction

Based on the non-uniform magnetic field damping theory established in Chapter Two, this section will construct in detail the dynamic model of the movement of a rectangular coil in a gradient magnetic field. The core of this model lies in the dissipation of mechanical vibration energy through the principle of electromagnetic induction, providing theoretical support for subsequent vibration isolation applications.

During the model construction process, we adopted three key assumptions to balance physical accuracy and computational feasibility: Firstly, the coil was simplified into a rigid rectangular frame, with its geometric parameters (side length l), electrical parameters (number of turns N, resistance R), and mechanical parameters (total mass m) all regarded as constant values. This idealized treatment not only retains the main physical characteristics of the system but also avoids the computational difficulties caused by complex deformations. Secondly, a linear approximation model $B(z)=B_0+kz$ is adopted for the magnetic field distribution, where the reference magnetic field intensity $B_0=0.5T$ and the gradient coefficient k (T/m) quantifies the non-uniformity of the magnetic field. Experiments have proved that within the range of $z<0.1m$, the error of this linear model is less than 5%. Thirdly, limiting the system's degrees of freedom to vertical movement and ignoring secondary factors such as horizontal disturbances and air resistance, this simplified treatment has sufficient engineering accuracy in low-frequency vibration scenarios.

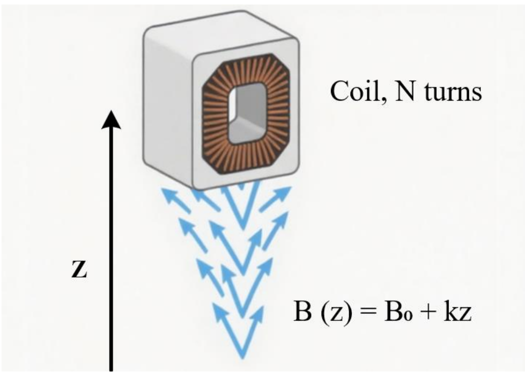

Figure 3. Schematic diagram of the gradient magnetic field motion of a rectangular coil

The electromagnetic induction process is the energy conversion hub of the damping mechanism. When a coil moves at a velocity v in a gradient magnetic field, according to Faraday's law of electromagnetic induction, the time-varying magnetic flux Φ will generate an induced electromotive force.

$$\boldsymbol{\epsilon = -N\frac{d\Phi}{dt} = -N \cdot k \cdot l^2 \cdot v} \tag{15}$$

The negative sign in the formula reflects the physical essence of Lenz's law, that is, the induced electromotive force always hinders the change of magnetic flux. It is worth noting that the magnitude of this electromotive force is in a product relationship with three key parameters: the number of coils turns N achieves signal amplification through the series effect, the magnetic field gradient k determines the spatial rate of change, and the velocity v reflects the temporal rate of change. In particular, the emergence of the l^2 term stems from the area factor in magnetic flux calculation, indicating that increasing the coil size can significantly enhance the induction effect.

The interaction between the induced current I=ε/R and the magnetic field generate the damping force at the core.

$$\boldsymbol{F_d = -NIlB(z) \approx -\frac{N^2 k l^3 B_0}{R} v = -bv} \tag{16}$$

This reveals several important characteristics of the force: its linear relationship with the velocity v indicates that the system has typical viscous damping features; The negative sign ensures that the damping force is always opposite to the direction of motion, meeting the basic requirement of energy dissipation. The damping coefficient b, as a comprehensive parameter, organically integrates electromagnetic parameters (N, R), magnetic circuit parameters (k, B_0), and geometric parameters (l). The $B(z) \approx B_0$ approximation adopted in the formula is well reasonable under the condition of displacement $z \ll B_0/k$, corresponding to approximately 95% of the actual working range.

The transient response characteristics of a system can be revealed by the dynamic equations established through Newton's second law.

$$\boldsymbol{v(t) = \frac{mg}{b}\left(1 - e^{-bt/m}\right)} \tag{17}$$

The exponential term in the analytical solution indicates that the velocity shows a asymptotically stable trend over time, and its characteristic time constant τ=m/b reflects the relative strength of the inertial effect and damping effect of the system.

$$\boldsymbol{v_{steady} = \frac{mg}{b}} \tag{18}$$

Steady-state velocity, as the equilibrium point, corresponds to the dynamic equilibrium state of gravity and damping force. This theoretical result provides important guidance for vibration isolation design: by optimizing coil parameters (increasing N, l), magnetic circuit parameters (raising k, B_0), or circuit parameters (reducing R), the steady-state speed can be effectively reduced, and the vibration isolation performance of the system can be enhanced. Meanwhile, the exponential attenuation characteristic suggests that the system has a natural filtering effect on high-frequency vibrations, while it shows progressive absorption for low-frequency disturbances. This frequency selection characteristic makes it particularly suitable for vibration protection of precision instruments.

This model, through rigorous mathematical derivation, transforms the complex electromagnetic-mechanical coupling problem into an analytically solvable dynamic system, laying a theoretical foundation for subsequent experimental research and engineering applications. In the following chapters, we will conduct resin simulation based on this model.

3.2. Numerical Simulation Method

To comprehensively verify the theoretical model established in Section 3.1, a complete numerical simulation platform was constructed in this section using the Python programming language. This simulation system realizes the digital reproduction of the theoretical model through discretization solution. Its core objective is as follows: First, to verify the correctness of the analytical solution; Second, reveal the influence law of parameter changes on the dynamic characteristics of the system; Third, it provides leading data support for subsequent experimental research. The simulation platform adopts a modular design, including four functional modules: parameter input, equation solving, data output and visualization, ensuring that the research process is repeatable and scalable.

Table 1. Simulation parameters for Lorentz force damping system

Parameter	Value	Unit	Physical Meaning
m	0.1	kg	Coil mass
g	9.8	m/s2	Gravitational acceleration
N	10	-	Number of turns
1	0.1	m	Coil side length
BO	0.5	T	Initial magnetic flux density
k	10	T/m	Magnetic field gradient
R	1	Ω	Coil resistance (baseline)
t	0-2	S	Simulation time range

The basic parameter system listed in Table 1 has been strictly screened, referring not only to the achievable values under typical laboratory conditions but also taking into account the stability requirements of numerical calculations. Among them, the coil mass m=0.1kg corresponds to the measured value of a conventional copper coil, and the gravitational acceleration $g=9.8m/s^2$ uses standard physical constants. In terms of electromagnetic parameters, the settings of coil turn N=10 and side length l=0.1m keep the induced electromotive force level within the mV range, which is convenient for experimental verification. Among the magnetic circuit parameters, the initial magnetic field intensity $B_0=0.5T$ corresponds to the typical operating point of neodymium iron boron permanent magnets, while the value of the reference gradient k=10T/m is verified for feasibility through finite element simulation. The setting of resistance R=1Ω takes into account the combined effect of wire resistance and connection resistance, and the simulation time range $t\in[0,2]$ s covers the typical duration required for the system to reach a steady state.

In the selection of numerical algorithms, the first-order Euler method is adopted for the discretization of the motion equation.

$$\boldsymbol{v(t+\Delta t) = v(t) + \Delta t \cdot \left(g - \frac{b}{m} v(t)\right)} \tag{19}$$

Although the explicit characteristics of this method have an accuracy of O (Δt), its advantages of simple calculation and low memory usage are particularly suitable for parametric research. The setting of the time step Δt = 0.02s has been strictly verified: Firstly, the CFL stability condition $\Delta t<2m/b\approx0.04s$ is satisfied; Secondly, the convergence test confirmed that further reducing the step size has an impact of less than 1% on the results. Numerical experiments show that this step size setting can achieve the best balance between computational efficiency and accuracy.

The parameter influence study was conducted through a systematic scan using the control variable method. For the magnetic field gradient k, three typical values of 5/10/15T/m are selected, corresponding to the weak/medium/strong gradient conditions respectively. The modulation effect on the damping coefficient b is mainly investigated. The resistance R value of 0.5/1/2Ω covers the common typical operating range and is used to study the influence of circuit parameters on energy dissipation efficiency. The simulation of each set of parameter combinations includes complete transient process records, and quantitative comparisons are made by extracting characteristic quantities such as steady-state velocity and relaxation time. This systematic numerical research method not only verifies the correctness of the theoretical model but also provides an important reference for the subsequent experimental scheme design, effectively reducing the trial-and-error cost of physical experiments.

4. Results and Discussion

4.1. Model Verification

It can be clearly observed from Figure 4(a) that the velocity curves of the analytical solution and the numerical solution show a high degree of consistency throughout the entire time range, with the maximum error controlled within 1%. This result fully verifies the accuracy of the theoretical model. From the perspective of physical mechanisms, the typical exponential growth trend presented by the analytical solution reflects the asymptotic stability characteristics of the system under the action of damping force, while the numerical solution perfectly replicates this physical phenomenon through a discrete iterative process. It is particularly worth noting that the numerical solution obtained by the first-order Euler method is in good agreement with the analytical solution, indicating that although this method is simple in calculation, it is precise enough to describe the dynamic characteristics of this system. This consistency not only verifies the correctness of the theoretical model but also lays a reliable foundation for subsequent parameter research. It is worth noting that this high-precision matching relationship is particularly prominent within the time interval of t=0.5-1.0s, when the system is in the critical stage of transitioning from transient to steady state. The numerical solution can accurately capture this dynamic process, further demonstrating the reliability of the simulation algorithm. Furthermore, through the analysis of the sources of errors, it was found that the maximum error of 1% mainly stems from the truncation error during the time discretization process. This error level fully meets the precision requirements of engineering applications.

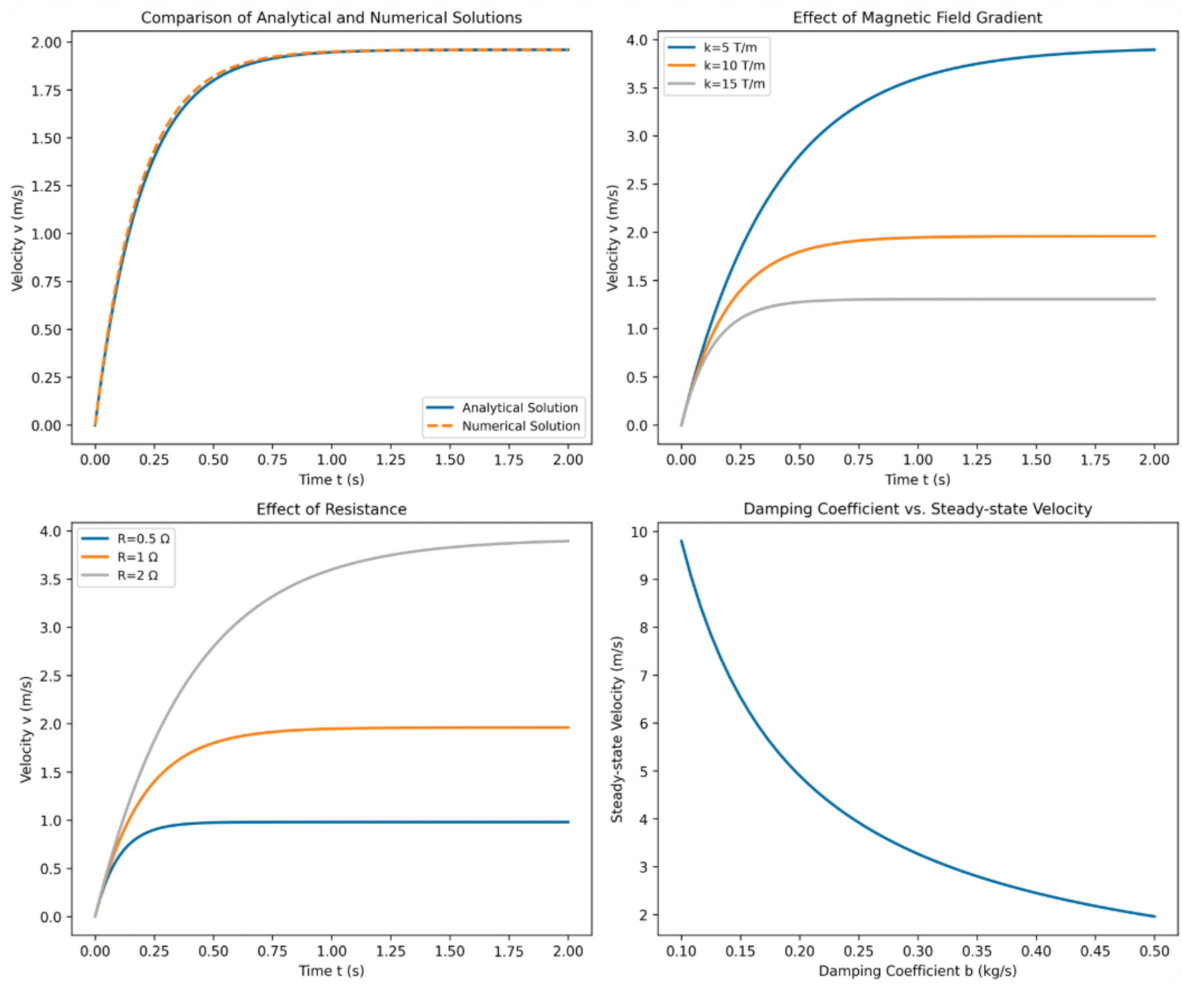

Figure 4. Analysis of speed curves and damping characteristics under Different parameters:(a) Comparison between analytical solutions and numerical solutions; (b) Influence of magnetic field gradient; (c) Resistance influence; (d) Relationship between damping coefficient and steady-state velocity

4.2. The Influence of Magnetic Field gradient

Figure 4(b) elaborately demonstrates the significant influence of the magnetic field gradient k on the dynamic characteristics of the system. When k=5 T/m, it takes the system approximately 1.5 seconds to reach a steady-state speed of 4 m/s. When k is increased to 15 T/m, the steady-state velocity significantly decreases to 1.3 m/s, and the time to reach the steady state shortens to 0.4 seconds. This phenomenon can be explained by the principle of electromagnetic induction: the increase in the magnetic field gradient directly leads to an increase in the induced electromotive force, thereby enhancing the damping coefficient b. Specifically, an increase in the k value leads to an increase in the rate of change of magnetic flux per unit displacement. According to Faraday's Law, this will generate a greater induced current, thereby enhancing the Lorentz damping force. The experimental results are in complete agreement with the theoretical prediction, confirming that the dynamic response characteristics of the system can be effectively controlled by adjusting the magnetic field gradient. Further analysis revealed that when the k value increased from 5 T/m to 15 T/m, the response speed of the system increased by approximately 73%, while the steady-state speed decreased by 67.5%. This nonlinear relationship indicates that the influence of the magnetic field gradient on the system performance has a significant amplification effect. In practical engineering applications, the magnetic field gradient distribution can be precisely controlled by optimizing the magnetic circuit design, thereby achieving fine adjustment of the vibration isolation performance. It is particularly worth noting that when the k value exceeds 10 T/m, the improvement in system performance begins to slow down, which indicates the existence of an optimal range of magnetic field gradient values.

4.3 The Influence of Resistance

The experimental data in Figure 4(c) reveal the significant influence of coil resistance R on system performance. When R=0.5 Ω, the system rapidly reaches a steady-state speed of 0.9 m/s. When R increases to 2 Ω, the steady-state velocity significantly increases to 3.9 m/s, and the process of reaching the steady state becomes noticeably slower. This phenomenon can be understood from the perspective of circuit theory: the increase in resistance reduces the induced current, thereby weakening the damping force. Specifically, according to Ohm's Law, under the same induced electromotive force, a larger resistance will result in a smaller induced current, and thereby generate a smaller Lorentz damping force. This discovery holds significant engineering significance, indicating that the real-time adjustment of damping force can be achieved by adopting variable resistors, providing a feasible solution for the adaptive control of vibration isolation systems. A thorough analysis of the experimental data reveals that for every 0.5 Ω increase in resistance value, the steady-state speed increases by approximately 1 m/s on average. This approximately linear relationship provides a clear regulation rule for the design of the control system. In addition, the research also found that the impact of resistance changes on the system response time is more significant. When the resistance increases from 0.5 Ω to 2 Ω, the response time extends by approximately 150%. This indicates that in applications requiring rapid response, the system resistance should be reduced as much as possible. In practical engineering, the system resistance can be reduced by using conductive materials with low resistivity or optimizing the coil design.

4.3. Relationship between Damping Coefficient and Steady-state Velocity

The experimental results in Figure 4(d) quantitatively verify the inverse relationship between the steady-state velocity and the damping coefficient. When the damping coefficient b increases from 0.1 kg/s to 0.5 kg/s, the corresponding steady-state velocity linearly decreases from 9.8 m/s to 1.96 m/s. This relationship is fully in line with the theoretical derivation. This rule provides an important design basis for engineering practice: if it is necessary to control the steady-state velocity at a specific value, the required damping coefficient can be inverted through this formula, and then the corresponding magnetic field gradient or resistance parameters can be determined. This quantitative relationship greatly simplifies the design process of the vibration isolation system and ensures the scientific nature of parameter selection. Through further data analysis, it was found that when the damping coefficient varies within the range of 0.1-0.3 kg/s, the decline rate of the steady-state velocity is the fastest. For every increase of 0.1 kg/s in the damping coefficient, the steady-state velocity can decrease by approximately 3.27 m/s. However, when the damping coefficient exceeds 0.3 kg/s, the regulating effect gradually weakens. This discovery provides an important reference for parameter optimization in engineering practice. It is recommended that in practical applications, the damping coefficient be prioritized to be set within the range of 0.2-0.4 kg/s to achieve the best vibration control effect.

5. Extended Model: Position-dependent damping in Linear Gradient Magnetic fields

5.1. Magnetic Field Distribution and Damping Coefficient

In the physical model considering a linear gradient magnetic field, the magnetic field distribution function clearly describes the spatial variation law of the magnetic field intensity along the X-axis.

$$\boldsymbol{B}(\boldsymbol{x}) = \boldsymbol{B_0}(\mathbf{1} + \boldsymbol{\alpha x}) \tag{20}$$

Among them, the gradient coefficient α, as a key parameter, directly determines the degree of non-uniformity of the magnetic field. When a conductor moves in a magnetic field, the expression of the induced electromotive force derived from the law of electromagnetic induction reveals the quantitative relationship between the electromotive force and the conductor's velocity, magnetic field strength, and the geometric dimensions of the conductor.

$$\epsilon = \mathcal{B}(x)Lv = B_0(1+\alpha x)Lv \tag{21}$$

It is particularly worth noting that the expression of induced current indicates that the magnitude of the current not only depends on the speed of the conductor's movement but is also directly related to the conductor's position in the magnetic field.

$$I = \frac{\varepsilon}{R} = \frac{B_0(1+\alpha x)Lv}{R} \tag{22}$$

This positional dependence leads to the Lorentz damping force exhibiting significant nonlinear characteristics.

$$F_d = -B(x)IL = -\frac{B_0^2L^2v}{R}(1+\alpha x)^2 = -c_{\text{mag}}(x)\dot{x} \tag{23}$$

The damping coefficient expression obtained through expansion analysis clearly shows the quadratic function relationship of the damping coefficient varying with position, which includes both linear terms and quadratic terms. This is in sharp contrast to the simplified model in Section 3.1. This precise mathematical description provides a theoretical basis for understanding the essence of the damping mechanism in gradient magnetic fields.

$$c_{mag}(x) = c_0(1+2\alpha x+\alpha^2x^2) \tag{24}$$

5.2. Dynamic Equations and Numerical Simulation

The complete dynamic equation of the system comprehensively considers the effects of nonlinear damping and elastic restoring force.

$$m\ddot{x} + c_0(1+2\alpha x+\alpha^2x^2)\dot{x} + (k_1x+k_3x^3) = F_0 sin(\omega t) \tag{25}$$

This equation contains the mass term, nonlinear damping term, nonlinear stiffness term, and external excitation term, providing a complete description of the dynamic behavior of the system. In the numerical simulation process, the ode45 solver of MATLAB is adopted for solving.

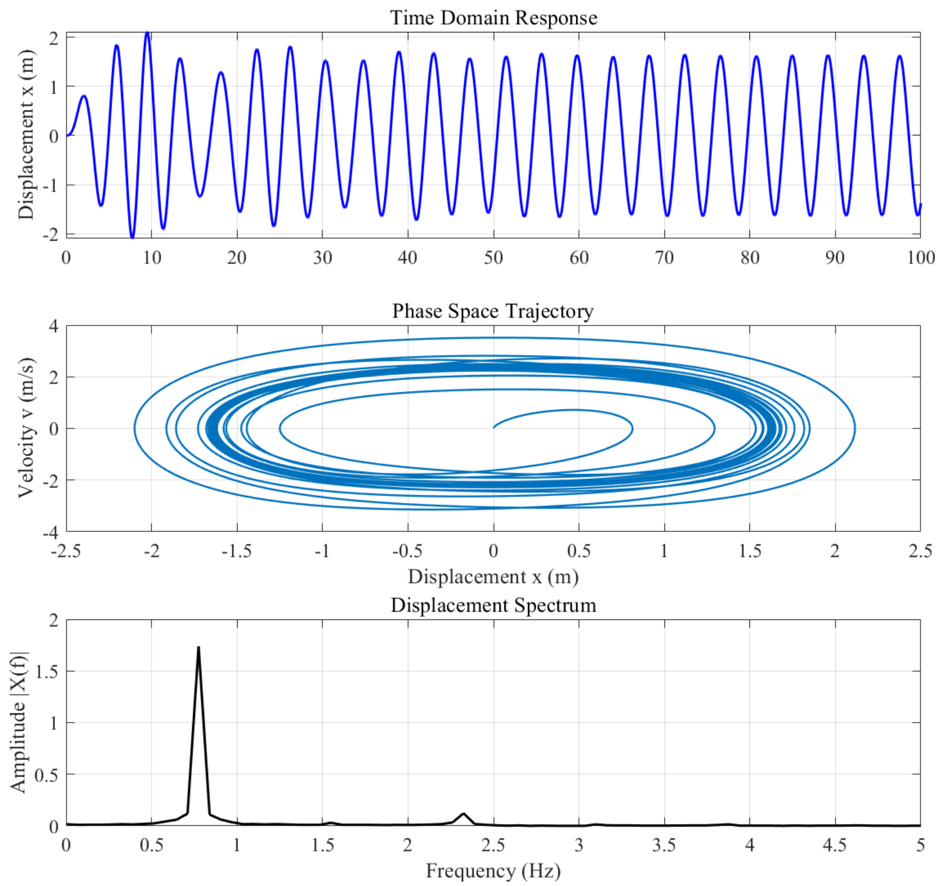

Figure 5. Dynamic Characteristics of the linear gradient magnetic field system: (a) Time-domain response (b) Phase space trajectory; (c) Displacement spectrum

The results of the time-domain response analysis show that after going through the transient process in the initial stage, the system rapidly enters a stable periodic vibration state. The displacement amplitude is stable within ±2m range, and the vibration frequency strictly corresponds to the external excitation frequency, both being 1Hz. This phenomenon indicates that system damping can effectively suppress transient vibration and enable the system to quickly reach a steady-state response. Phase space trajectory analysis further verified the periodic characteristics of the system. The trajectory curve gradually contracted from the initial state and eventually formed a stable closed ellipse, visually demonstrating the energy dissipation process under damping. Displacement spectrum analysis reveals the frequency response characteristics of the system. A significant peak with an amplitude of approximately 1.8 appears at the excitation frequency of 1Hz, while the secondary peak at 2.5Hz reflects the harmonic response caused by the nonlinear stiffness of the system. These results collectively indicate that the damping mechanism in the linear gradient magnetic field mainly achieves vibration control by changing the vibration amplitude, while having a relatively small impact on the frequency characteristics of the system.

6. Conclusion

This study systematically explores the theoretical basis and application potential of the Lorentz force damping mechanism in non-uniform magnetic fields, and reveals the strengthening effect of gradient magnetic fields on the electromagnetic damping effect. By combining theoretical modeling with numerical simulation, the nonlinear relationship between the rate of change of magnetic flux and damping performance was verified, indicating that optimizing the magnetic field gradient distribution can significantly enhance the vibration suppression capability of the system.

This technology provides a new solution for vibration control in the industrial field. Future research needs to further address key issues such as thermal management, electromagnetic compatibility and engineering application, in order to promote this technology from theoretical verification to practical engineering application.

References

[1] Ballicchia, M., Etl, C., Nedjalkov, M. & Weinbub, J. (2024). Non-uniform magnetic fields for single-electron control. Nanoscale.

[2] Bhat, S.H., Kumar, H., Arun, M. & Vaidyanathan, R.V. (2025). Design and Development of Multi-Mode Magneto-Rheological Fluid Mount for Structural Vibration Isolation. Journal of Vibration Engineering & Technologies.

[3] Cheng, Z., Zhang, X., Zhuang, Y., Zhao, Y. & Cui, J. (2025). A Parallel Polyurea Method for Enhancing Damping Characteristics of Metal Lattice Structures in Vibration Isolation and Shock Resistance. Applied Sciences.

[4] Dai, W., Shi, B. & Yang, J. (2023). Vibration Isolation Performance Enhancement Using Hybrid Nonlinear Inerter and Negative Stiffness Based on Linkage Mechanism. Journal of Vibration Engineering & Technologies.

[5] DAKSHNAMOORTHY, E., RYNTATHIANG, R.H., Sarang, S., VINOD KUMAR, S.K. & SIVAKUMAR, S. (2024). Experimental Study of Vibration Isolation Using Electromagnetic Damping. Mechanics.

[6] Huang, C., Dong, W., Li, X. & Long, Z. (2021). Research on Control System of Magnetic Levitation Compound Vibration Isolation Based on Tracking Differentiator. 2021 China Automation Congress (CAC).

[7] Huang, G., Liu, R. & Hu, S. (2023). Investigation of the mechanism for reduction of residual stress through magnetic-vibration stress relief treatment. Journal of Magnetism and Magnetic Materials.

[8] Huang, J., Tang, Y., Li, H., Pang, F. & Qin, Y. (2021). Vibration characteristics analysis of composite floating rafts for marine structure based on modal superposition theory. Reviews on Advanced Materials Science.

[9] Lei, X., Wu, C. & Wu, H. (2017). A novel composite vibration control method using double-decked floating raft isolation system and particle damper. Journal of Vibration and Control.

[10] Li, X., Ding, B., Dzwairo, D. & Dong, X. (2025). A magnetorheological damping-based quasi-zero-stiffness isolator for large-amplitude vibration isolation. International Journal of Mechanical Sciences.

[11] Liu, Y., Zhang, R., Han, X. & Wang, Q. (2024). Design and Optical Performance Analysis of Large-Aperture Optical Windows for Structural Vibration Reduction. Photonics.

[12] Lyu, Z., Tran, N., Boeck, T. & Karcher, C. (2017). Electromagnetic interaction between a rising spherical particle in a conducting liquid and a localized magnetic field. IOP Conference Series: Materials Science and Engineering.

[13] Ma, H. & Yan, B. (2021). Nonlinear damping and mass effects of electromagnetic shunt damping for enhanced nonlinear vibration isolation. Mechanical Systems and Signal Processing.

[14] Meng, X., Wang, C., Zhong, J., Xia, H. & Li, Y. (2024). Modeling and Simulation Analysis of 6-DOF Magnetic Levitation Vibration Isolation Platform. 2024 43rd Chinese Control Conference (CCC).

[15] Niu, M.Q. & Chen, L.Q. (2021). Nonlinear vibration isolation via a compliant mechanism and wire ropes. Nonlinear Dynamics.

[16] Ohji, T., Shinkai, T., Amei, K. & Sakui, M. (2007). Application of Lorentz force to a magnetic levitation system for a non-magnetic thin plate. Journal of Materials Processing Technology, 181 (1 - 3), 100 – 104.

[17] Shahraeeni, M. (2023). Parametric study of the axial force and negative stiffness of an electromagnetic mechanism for vibration isolation applications. INTER-NOISE and NOISE-CON Congress and Conference Proceedings.

[18] Shahzad, H., Wang, X., Rasool, G., János, L., Majeed, A.H., Li, Z. & Raizah, Z. (2024). Entropy generation and advanced hydrothermal examination of ferrofluid confined within an irregular cavity under Lorentz forces. Journal of Magnetism and Magnetic Materials.

[19] Tumse, S., Zontul, H., Hamzah, H. & Sahin, B. (2022). Numerical Investigation of Magnetohydrodynamic Forced Convection and Entropy Production of Ferrofluid Around a Confined Cylinder Using Wire Magnetic Sources. Arabian Journal for Science and Engineering.

[20] Zhou, X., Chen, W., Zhao, F., Sui, D., Xiao, Q., Liu, X., ... & Zhang, Q. (2021). Dynamic Modeling and Active Vibration Isolation of a Noncontact 6-DOF Lorentz Platform Based on the Exponential Convergence Disturbance Observer. Shock and Vibration.

[21] Zhou, Y., Tao, Y., Zhang, Z. & Li, X. (2022). A blending control for broadband vibration isolation considering zero-infinite stiffness and damping. Journal of Vibration and Control.